

Contents lists available at ScienceDirect

Journal of Energy Chemistry



journal homepage: www.elsevier.com/locate/jechem

Protein-modified SEI formation and evolution in Li metal batteries

Chenxu Wang, Ryan Odstrcil, Jin Liu*, Wei-Hong Zhong*

School of Mechanical and Materials Engineering, Washington State University, Pullman, WA 99164, USA

ARTICLE INFO

Article history: Received 26 April 2022 Revised 1 June 2022 Accepted 9 June 2022 Available online 18 June 2022

Keywords: Protein Zein Lithium metal Stand-still Battery SEI

ABSTRACT

Despite numerous reported lithium metal batteries (LMBs) with excellent cycling performance achieved in labs, transferring the high performing LMBs from lab-scale to industrial-production remains challenging. Therefore, via imitating the stand-still process in battery production, a conventional but important procedure, to investigate the formation and evolution of a solid electrolyte interface (SEI) is particularly important for LMBs. Our previous studies indicate that zein (corn protein)-modified carbonate-ester electrolyte (the most commercialized) effectively improves the performance of LMBs through guiding Li-ions and repairing cracked SEI. Herein, we investigate the formation and evolution of the protein-modified SEIs on Li anodes by imitating the stand-still temperature and duration. A simulation study on the protein denaturation in the electrolyte under different temperatures demonstrates a highly unfolded configuration at elevated temperatures. The experiments show that this heat-treated-zein (H-zein) modified SEI forms quickly and becomes stable after a stand-still process of less than 100 min. Moreover, the Hzein SEI exhibits excellent wetting behavior with the electrolyte due to the highly unfolded protein structures with more functional groups exposed. The Li|Li cell with the H-zein SEI achieves prolonged cycling performance (>360 h vs. \sim 260 h of the cell with the untreated-zein (U-zein) modified SEI). The LiFePO₄|Li cell with the H-zein SEI shows much stable long-term cycling performance of capacity retention (70% vs. 42% of the cell with U-zein SEI) after 200 cycles. This study confirms that the appropriately treated protein is able to effectively improve the performance of LMBs, and will inspire future studies for the production process of LMBs toward their commercialization.

© 2022 Science Press and Dalian Institute of Chemical Physics, Chinese Academy of Sciences. Published by ELSEVIER B.V. and Science Press. All rights reserved.

1. Introduction

Numerous successful lab studies on achieving safe and long-term-cycling Li metal batteries (LMBs) have been reported [1]. However, transferring these high performing LMBs from lab-scale to industrial-production remains challenging [2]. Most of the lab studies on LMBs are limited to solving the issue of Li dendrite formation by an *in-situ* or *ex-situ* formed layer on Li anodes [3], while the formation and evolution of the SEI through imitating the practical production process of LMBs are rarely considered. The conventional production processes of batteries are divided into three main procedures: electrode manufacturing, cell assembly and cell finishing [4,5]. In the cell assembly process, the temperature and duration of the stand-still process after electrolyte filling are critical to the chemical reactions between electrodes and electrolyte. As we know, a metallic Li anode is chemically reactive to nearly all organic compounds [6]. When a liquid electrolyte is filled into

E-mail addresses: jin.liu2@wsu.edu (J. Liu), katie_zhong@wsu.edu (W.-H. Zhong).

LMBs, a passivation SEI layer forms by the immediate chemical reactions on the surface of Li, and the SEI layer has the function of decreasing the interface reactions. Over time, the SEI grows thicker and is able to suppress the further reactions before cycling [7]. However, a thick SEI (e.g., thickness >2 nm) leads to the large resistance of batteries [8]. Therefore, it is important to control the formation and evolution of SEI during the stand-still process after the electrolyte-filling procedure in the production of LMBs.

Thus far, many fundamental studies of SEI focused on its evolution after cell assembly, and most of them were based on the commercial graphite anode in Li ion batteries (LIBs) [7,9-12]. For example, the evolution of SEI during the long stand-still process after cell finishing was studied in different aging conditions such as storage temperature and states of charge in LIBs [13]; the chemical and electrochemical evolution of SEI during the cycling process was investigated to build the correlation between SEI and cycling performance [12,14,15]. In addition, in electrolyte systems with functional additives for SEI formation, the participation of additives in initial SEI formation was greatly impacted by the reaction condition parameters in the stand-still process after electrolyte

^{*} Corresponding authors.

filling [16,17]. However, there is a lack of reported work on the SEI formation and evolution in the cell assembly process of LMBs even though the work is highly demanded the practical production of LMBs.

Another factor critical to the SEI formation during the stand still process after electrolyte filling is the wetting behavior of electrolyte on electrodes of batteries, which is widely measured in the industry [18,19]. Within the conventional production processes of batteries, one of the most time-consuming procedures is the stand-still for reaching good wetting between electrodes and electrolyte after electrolyte filling. Typically, a complete wetting for good SEI formation in the filled batteries usually needs a stand-still duration of as long as several hours depending on the cell dimensions, capacities and the electrode components. Therefore, a study of wetting behavior is necessary for the control of SEI formation and evolution in the industrial production processes of batteries.

In our previous study, we investigated a protein additive for the widely commercialized carbonate-ester electrolytes to protect Li anodes [20]. Natural proteins are biopolymers composed of various amino acids with abundant functional groups (-CO-NH-, -COOH, -OH, -NH₂, etc.) that hide in quaternary structures [21]. With an appropriate denaturation process by thermal and/or salt treatments, quaternary or tertiary structures of the protein chains are unfolded due to the disruption of the weak forces (e.g., hydrogen bonds, disulfide bonds, salt bridges, etc.) [22,23]. It is found that the zein additive not only facilitates a uniform Li-ion flux to suppress the formation of Li dendrites, but also repairs the destroyed SEI to protect Li anodes from the continuous etching of carbonate-ester electrolyte. Specifically, we found that the formation and evolution of SEI is closely related to the formation time and temperature of the stand-still process after electrolyte filling, which has not yet been studied.

Here, through experiments and molecular simulations, we report a study on the formation of protein-modified SEIs on Li anodes at different stand-still temperatures, and their evolution is further investigated by controlling the duration of the standstill process. In particular, the evolution of SEI chemical components and wetting behavior of the SEI with the electrolyte are studied by controlling the conditions of the stand-still process. It is found that heat treatment used for protein denaturation leads to more unfolded chain structures, which is confirmed by the simulation study. The resulting heat-treated-zein (H-zein) modified SEI shows better wetting behavior with electrolyte and a quicker SEI formation than the unheated sample (denoted as U-zein). In addition, the symmetrical Li|Li cell with H-zein SEI shows a more prolonged cycle life of 360 h from 260 h for the counterpart with Uzein SEI. Moreover, the symmetrical LiFePO₄|Li cell with H-zein SEI presents a more stable long-term cycling performance with a capacity retention of 70% compared to 42% of the cell with Uzein after 200 cycles.

2. Experimental

2.1. Raw materials

Li metal circuit plates (\emptyset 15.8 mm) with a thickness of 250 μ m were purchased from China Energy Lithium Co., Ltd. The carbon ester electrolyte purchased from Sigma-Aldrich Co., Ltd is composed of 1.0 M LiPF₆ and ethylene carbonate/ethyl methyl carbonate (EC/EMC) (1:1 by volume). Zein was purchased from Sigma-Aldrich Co., Ltd (Purity >90%). The electrode components of LiFePO₄, carbon-coated Al foil, separator (Celgard 2400), super C45 and polyvinylidene fluoride binder (PVDF) were purchased from MTI Co., LTD.

2.2. Samples preparation

The preparation of the Li metal with various SEI layers was performed in an Ar-filled glovebox with water and oxygen content below 0.5 ppm. The electrolyte with zein content of 0.05 wt% was prepared by a dilution method. To prepare the Li metal with heat-treated-zein (H-zein) modified SEI, the electrolyte with zein was heated to 50 °C for 1 h and was coated on the surface of Li metals. Thereafter, the coated Li metals were dried and rinsed by 1,2-dimethoxyethane (DME) for three times. Untreated-zein (U-zein) modified SEI was prepared by the electrolyte with zein without heat treatment. For comparison, heat-treated-pure-electrolyte (H-pure) SEI and untreated-pure-electrolyte (U-pure) SEI were synthesized using pure electrolyte by the same procedure.

To investigate the evolution of SEI in stand-still process, the SEIs with different formation times were prepared by an *in-situ* method. Li metals were dipped into various electrolytes (with zein additive at 50 °C, with zein additive at 20 °C, pure electrolyte at 50 °C, pure electrolyte at 20 °C) for 1, 10, 100, 1000 min. Afterward, the Li metals were taken out of electrolytes and then were rinsed by DME for three times. The samples were collected for further characterization after dried.

2.3. Materials characterization

The morphologies of Li metal with various SEIs were characterized by SEM (Quanta 200F) and optical digital microscope (KEY-ENCE VHX-7000)). The Functional groups of SEIs were investigated by FTIR (Thermofisher iS10) using an ATR mode. FTIR-ATR was also employed to gain the functional groups on the pristine and cycled Li metal anodes in cells. The wetting behavior of electrolytes on various SEIs of Li metals was measured by an optical contact angle analyzer (OCA 15 plus, Dataphysics Instruments). The change of contact angle in 4 s was automatically recorded by the analyzer. Note that the contact angle testing of three substrates was in the same environment. The droplet volumes and drop speed were kept constant for each measurement of wetting behavior. The Raman laser excitation wavelength is 532 nm (4 cm⁻¹ spectral resolution) and the laser power was set to 1.2 mW. The exposure time of Raman is 0.33 s and averaged over 400 scans.

2.4. Electrochemical measurements

To test the electrochemical performance, the coin cell of LiFePO₄/Li and Li/Li cells were assembled. The assembling pressure was fixed at 100 MPa and the electrolyte amount was set to 40 μL for every coin cell. To fabricate LiFePO₄ electrode, LiFePO₄, super C45 and PVDF were mixed in *N*-methy-l-2-pyrrolidone (NMP) and stirred for 10 h. Then the uniform slurry was cast on the carbon-coated Al sheet and put into a vacuum oven for 12 h under 80 °C. The obtained electrode was punched into Ø12.7 mm discs, which have an average LiFePO₄ loading of \sim 7 mg cm $^{-2}$.

The symmetrical Li cell cells (Li|Li) were cycled within a voltage range of -0.5–0.5 V at various densities of 0.2, 0.5, 1 mA/cm². The cycling performance of LiFePO₄ half cells (Li|LiFePO₄) with the zein-modified electrolyte was tested by LAND multichannel battery cycler (Wuhan LAND Electronics Co., Ltd.) within a voltage range of 2.5–3.6 V (vs Li⁺/Li). The impedance of the resultant SEIs was measured through impedance spectroscopy (EIS) within a frequency range of 0.1– 10^6 Hz by an electrochemical workstation (BioLogic VSP).

2.5. Molecular dynamics simulations

Molecular dynamics simulations of the zein protein denaturation were performed with the GROMACS package (2020.3 version)

[24] with the OPLS force field [25]. The structural model of 19 kDa α -Zein (Z19) was used for the simulations. To set up the protein system, a single zein protein was centered in a periodic simulation box of size $12.7 \times 12.7 \times 12.7 \text{ nm}^3$ and was solvated with a 1:1 (v/ v) mixture of EC and EMC. The Li salt containing Li⁺ and PF₆ was added at a concentration of 1 mol/L. For both sets of simulations at 20 °C and 50 °C, the protein system was first minimized and then relaxed for 10 ns at the NVT and NPT ensembles using the associated temperature and a pressure of 1 bar. During the relaxation simulations, a velocity-rescaling thermostat and Berendsen barostat was used [26]. During the production simulations, a Parrinello-Rahman barostat was used [27]. The long-range Coulomb interactions were treated with the PME method and the Van der Waals interactions were handled with a 1.2 nm cutoff distance [28]. The simulated systems were visualized with VMD. The simulations were performed with a time step of 2 fs [29].

3. Results and discussion

3.1. Mechanism and properties of the protein-modified SEIs

In this work, we explore the formation and evolution of proteinmodified SEIs during the stand-still process at different temperatures and rationally control the molecular structure of zein by the simulation to form an SEI that suppresses the growth of Li dendrites [30]. Natural zein has complex macromolecules with a quaternary structure that is composed of closely packed arrangements of peptides. Sodium dodecyl sulphate-polyacrylamide gel electrophoresis (SDS-PAGE) is applied to analyze the molecular weight of protein. As shown in Fig. S1, the molecular weight of zein is determined to be 20–25 kDa (α , γ -zein) and 37–50 kDa (γ -zein). Fig. 1(a) depicts the concept and experimental process to control the protein molecular structure for creating protein-modified SEIs on Li anodes. To unfold the quaternary and tertiary structure, the denaturation of zein is carefully controlled, which has a great impact on Li-ion deposition. As shown, zein is firstly dissolved in carbon ester electrolyte and shows varied unfolding architecture at different temperatures. At the ambient temperature (20 °C), the macromolecules of zein are less unfolded, hiding numerous functional groups in the poorly unfolded structure. When in contact with Li anode, the poorly unfolded macromolecules exhibit a weak interaction with Li, generating an untreated-zein (denoted as U-zein) modified SEI with few exposed functional groups. In comparison, at the heat condition of 50 °C, the macromolecules of zein are more unfolded in electrolytes and expose abundant functional groups outside. When contacting with the Li metal, the strongly unfolded peptides generate stronger interactions with Li, forming a heat-treated-zein (denoted as H-zein) modified SEI. The H-zein SEI with rich exposed functional groups leads to an even Li-ion flux during the deposition process. Heat-treatedpure-electrolyte (denoted as H-pure) modified SEI and untreatedpure-electrolyte (denoted as U-pure) SEI are prepared as reference

A series of all-atom molecular dynamics (MD) simulations are performed to explore the structural change of zein in carbonate ester electrolyte at different temperatures. The simulation for the evolution of the zein structure with a time duration of 700 ns is illustrated in Fig. 1(b). The radius of gyration (Rg) is a fundamental parameter that characterizes the expansion of protein molecules. As shown, Rg of zein at the elevated temperature is about 2.60 nm at 200 ns and continually increases to 2.75 nm at 700 ns, whereas the Rg of zein at ambient temperatures is about 2.50 nm at 200 ns and 2.55 nm at 700 ns. The simulation shows that zein structure at ambient temperature is nearly unchanged compared to more unfolded zein at elevated temperature. The root

mean square deviation (RMSD) is a similarity measure that is widely applied in the structural analysis of proteins for the comparison between the structure of the natural fold and the unfolded protein structure (Fig. S2a). It can be seen that at ambient temperature, the protein unfold slowly to the RMSD of 0.3 nm in the time range of 0-40 ns, and then keep a nearly constant value after 40 ns (Video S1). For the zein at elevated temperature, the protein unfold rapidly to the RMSD value of 0.35 in the beginning of simulation and keep a constant slow unfold speed to 0.6 nm within the 200 ns (Video S2). The contact number of Li⁺ near polar residues on per protein molecule is further calculated to investigate the unfolded structure of protein in electrolyte (Fig. 1c). At ambient temperature, the zein molecule has a stable Li⁺ contacts of 23 between 70 ns to 600 ns, while at the elevated temperature, the Li⁺ contacts increases from 15 (0 ns) to 40 (700 ns). The above simulations indicate that even though zein molecules are denatured in the carbonate ester electrolyte at both elevated and ambient temperatures, the molecular structure at an elevated temperature is more expanded and flexible than the molecules at ambient temperature (Fig. S2b and c). Based on the prevalence of increased Li⁺ ion interactions with the zein at the elevated temperature, the mechanism behind the denaturation of zein for this system appears to be a coupling between temperature effects and the polar interactions occurring between polar residues in zein and Li⁺. It is known that an increased temperature increases the fluctuations of molecular interactions and thereby weakens bonds in the protein structure. More polar residues become accessible because of the opening of the protein structure, allowing for more Li⁺ interactions with the polar residues. The Li⁺ that close to polar residues shields the residues from other polar residues in zein, further weakens the original protein bonds. Through this coupled mechanism of the increased temperature and inclusion of Li⁺ ions, the zein becomes more denatured. This simulation demonstrates the impact of temperature control during the stand-still process on the cells with protein-modified carbonate-ester electrolytes.

The scanning electron microscopic (SEM) images and optical microscope (with polarized light) images of various SEIs are compared in Fig. 2(a). Note that all of the treated Li anodes are rinsed by (1,2-dimethoxyethane) DME three times to remove Li salt. It can be seen that the U-pure and H-pure SEIs have the same morphology in which no clear layer can be distinguished from the surface of Li anodes compared to the pristine Li without treatment (Fig. S3). For the U-zein Li metal, a flat new zein-derived SEI can be found on the surface, indicating the reaction between zein and Li metal. In contrast, the H-zein Li metal has a lot of flocculent protein particles on top of H-zein SEI. This result can be ascribed to the strong interaction between strong unfolded protein macromolecules, which is induced by the heat treatment and is demonstrated in the simulation (Fig. 1).

To investigate the functional groups of various SEIs, Fouriertransform infrared spectroscopy (FTIR) is tested and is shown in Fig. 2(b). To eliminate the distractions of the rinse solvent (DME), the FTIR of pristine Li metals rinsed by pure DME both with and without heat-treating are tested as the reference samples (Fig. S4). In the high-frequency range, the bands of intermolecular hydrogen-bonding (O–H) appear at around 3590 cm⁻¹ after adding zein, which is not detected in pristine Li metal and pure zein (Fig. S5), indicating the denaturation of zein macromolecules in SEIs of H-zein and U-zein. Moreover, the intramolecular hydrogen-bonding (O-H) has three peaks at around 2849 cm⁻¹, which can be found to be disappearing in U-zein SEI while existing in other SEIs. This result may be due to the weak interaction between the unfolded protein and Li metal that leads to the flushout of unfolded protein molecules by DME from U-zein SEI, such that the remained partially-unfold-protein modified SEI effectively impedes the reactions between DME and Li metal. In comparison,

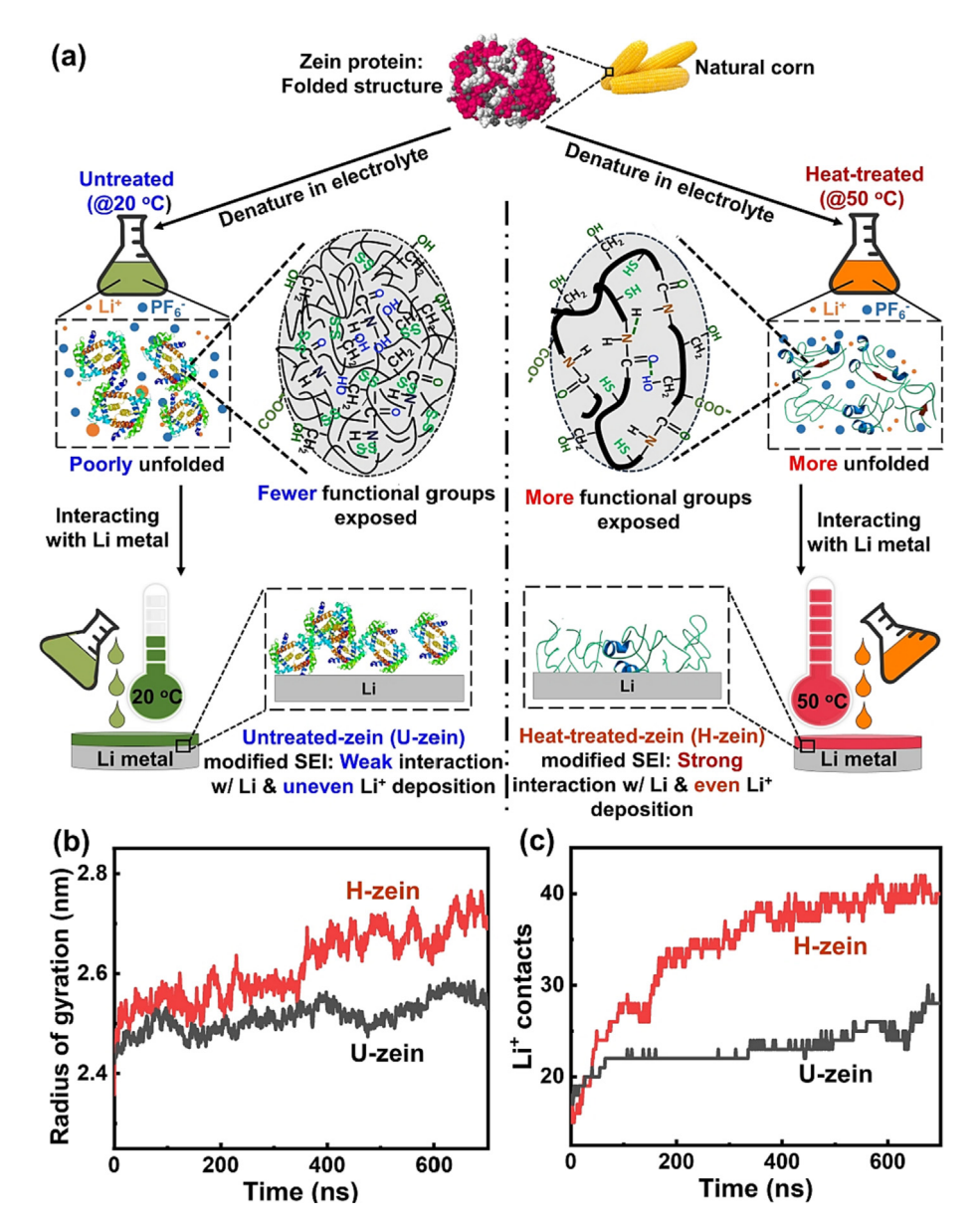


Fig. 1. (a) Schematic of tailoring the protein configurations to modify SEIs. The natural zein protein was denatured in carbon ester electrolyte at different temperatures. At 20 °C, zein molecules are poorly unfolded and have fewer functional groups exposed, resulting in an untreated-zein (U-zein) modified SEI that has weak interactions with the Li anode and induces an uneven Li⁺ deposition. At 50 °C, the heat-treated zein molecules are more unfolded and exposed to more functional groups, leading to the strong interactions between heat-treated-zein (H-zein) modified SEI and Li metals, and generating even Li-ion deposition. (b) The evolution of radius of gyration of zein in the electrolyte at different temperatures. (c) The evolution of the number of Li⁺ contacts with polar residues in the protein within 0.35 nm of zein molecules in the electrolyte at different temperatures.

the sharp peak of intramolecular hydrogen-bonding appeared in Hzein SEI. This is because of the strong unfolding structure of protein after being heat-treated and the abundance of strongly adhered zein particles on the SEI. In the low-frequency region, new peaks that correspond to new exposed functional groups (e.g., -C=O, C=N, C-N) are shown in U-zein and H-zein when compared to the U-pure and H-pure SEIs, representing the participation of protein in the formation of U-zein and H-zein SEIs (Table S6). Moreover, it can be seen that H-zein SEI shows more peaks than U-zein SEI, demonstrating the strongly unfolded state of the heat-treated protein that exposes abundant functional groups outside, which is also confirmed by Raman results (Fig. S18).

Dynamic contact angle measurement is conducted with pristine electrolytes on different SEIs to investigate the wetting behavior of the SEIs with electrolytes droplets (Fig. 3). Wetting behavior of electrolyte on Pure DME treated Li metals is tested as the reference

for various SEIs (Fig. S7). The measurement results that are repeatable and exhibit stable contact angles evolution are chosen for the study. All of the samples are tested in the same environment and the drop rate and drop volume are strictly controlled. For convenience, the results are divided into three domains as presented in Fig. S6 [31]. The first domain (rapid zone: from t_0 to t_1) is a sharp slope that shows a rapidly decreasing rate of contact angle. The second domain (transition zone: from t_1 to t_2) is characterized by a smaller slope which indicates a slow-spreading rate of the droplet. The third domain (static zone: after t_2) shows a constant value of contact angle in the ideal situation. As shown in Fig. 3, all of the four curves correspond to the typical curve of contact angle. In the rapid zone, it can be seen that H-zein SEI has the highest absolute value of slope (|k| = 57), which is due to the specific nanostructure of the surface with flocculent protein particles (Fig. 2a). H-pure SEI has the lowest absolute value of slope (|k| =16), which may be due

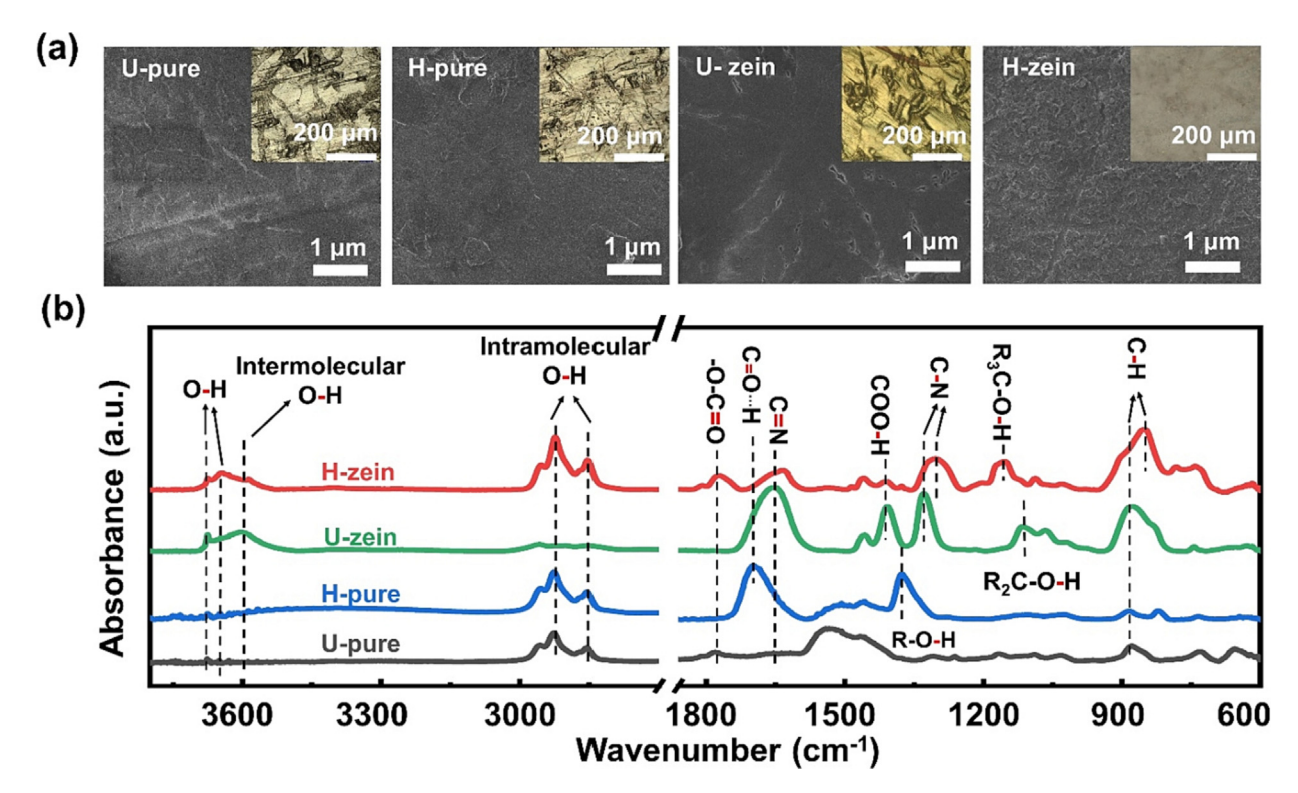


Fig. 2. SEM (a) and ATR-FTIR (b) results of Li anodes with various SEIs. Insert in (a): optical images of SEI under polarized light.

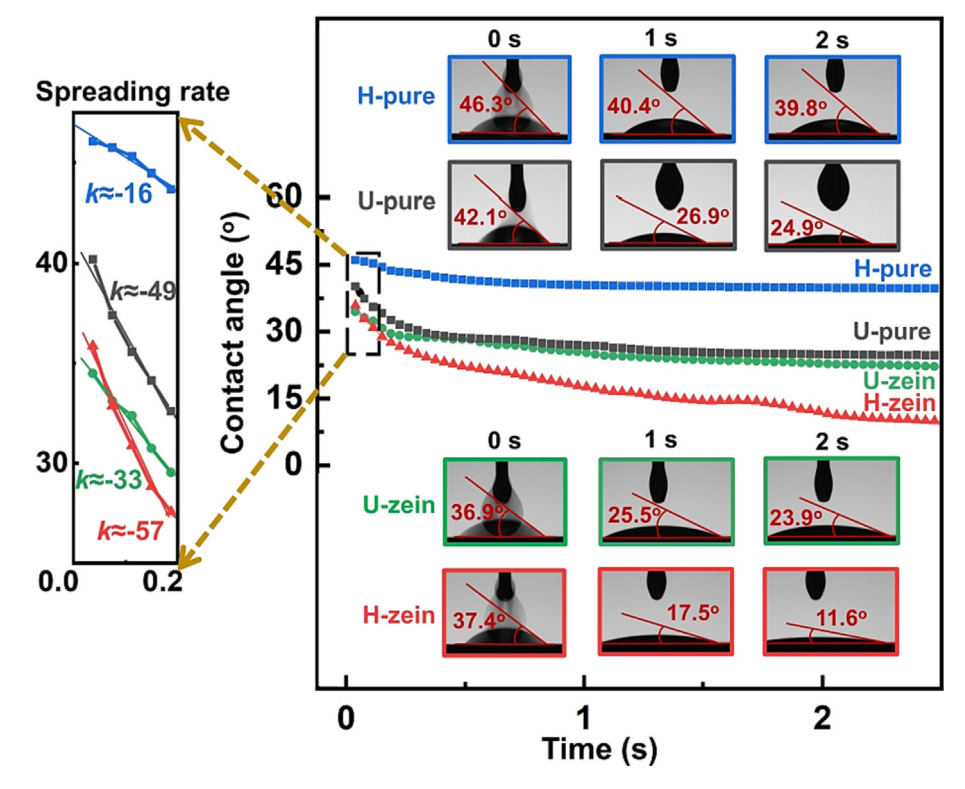


Fig. 3. Wetting behaviour of electrolyte on the Li metals with various SEIs.

to the thick pure-electrolyte-derived SEI with poor electrolyte wettability compared to the thin SEI of U-pure. At the initial state (0 s), the contact angle of U-pure, U-zein, H-zein and H-pure are 46.3°, 42.1°, 36.9° and 37.4°, respectively, and after 1 s of droplet spreading, the contact angles decrease to 40.4° , 26.9° , 25.5° and 17.5° ,

respectively. In the static zone, the contact angles of U-pure, U-zein, H-zein and H-pure maintain constant values of 39.8° , 24.9° , 23.9° and 11.6° , respectively. As a reference, the DME-derived SEIs with and without heat treatments (Fig. S7) have contact angles of 40.6° and 45.62° , respectively. These results confirm that the

heat-treated protein provides abundant exposed functional groups, forming a zein-derived SEI (H-zein) with abundant functional groups and protein nanoparticles that enhance the wettability of Li metals with electrolytes.

3.2. Evolution of the protein-modified SEI

A set of experiments are designed to investigate the evolution of protein modified SEIs with and without heat treatment at different formation time to imitate the stand-still process. As shown in Fig. 4(a), in the first step, Li metals are floated in various electrolytes (heat-treated and untreated with and without zein) for various time (1, 10, 100 or 1000 min) to form various SEI layers. Thereafter, the Li metals with an SEI layer are taken out from the electrolyte, rinsed, and dried in the glovebox for further character-

ization. The U-pure SEIs at various formation time are observed as the reference. As shown in Fig. S8, small particles can be found on Li surface at 1 min compared to the pristine Li (Fig. S3), these particles can be ascribed to the uneven dispersion of initial surface oxidation that induces the uneven reaction between Li and electrolyte. From 10 to 1000 min, it can be found that more particles forms, leading to a flatter and more condensed surface with the time. The SEM images of other SEIs at various formation time are shown in Fig. 4(b). For the H-pure SEI, the morphology at 1 min has no big difference with U-Pure SEI. However, a quicker formation of particles with loose packing can be found at 10 min for H-pure SEI, and generate a compact-packed SEI at 100 min and a rough SEI after 1000 min. This phenomenon demonstrates that elevated temperature improves the formation and growth of SEI particles. In comparison, for H-zein and U-zein SEIs, the evolution of a

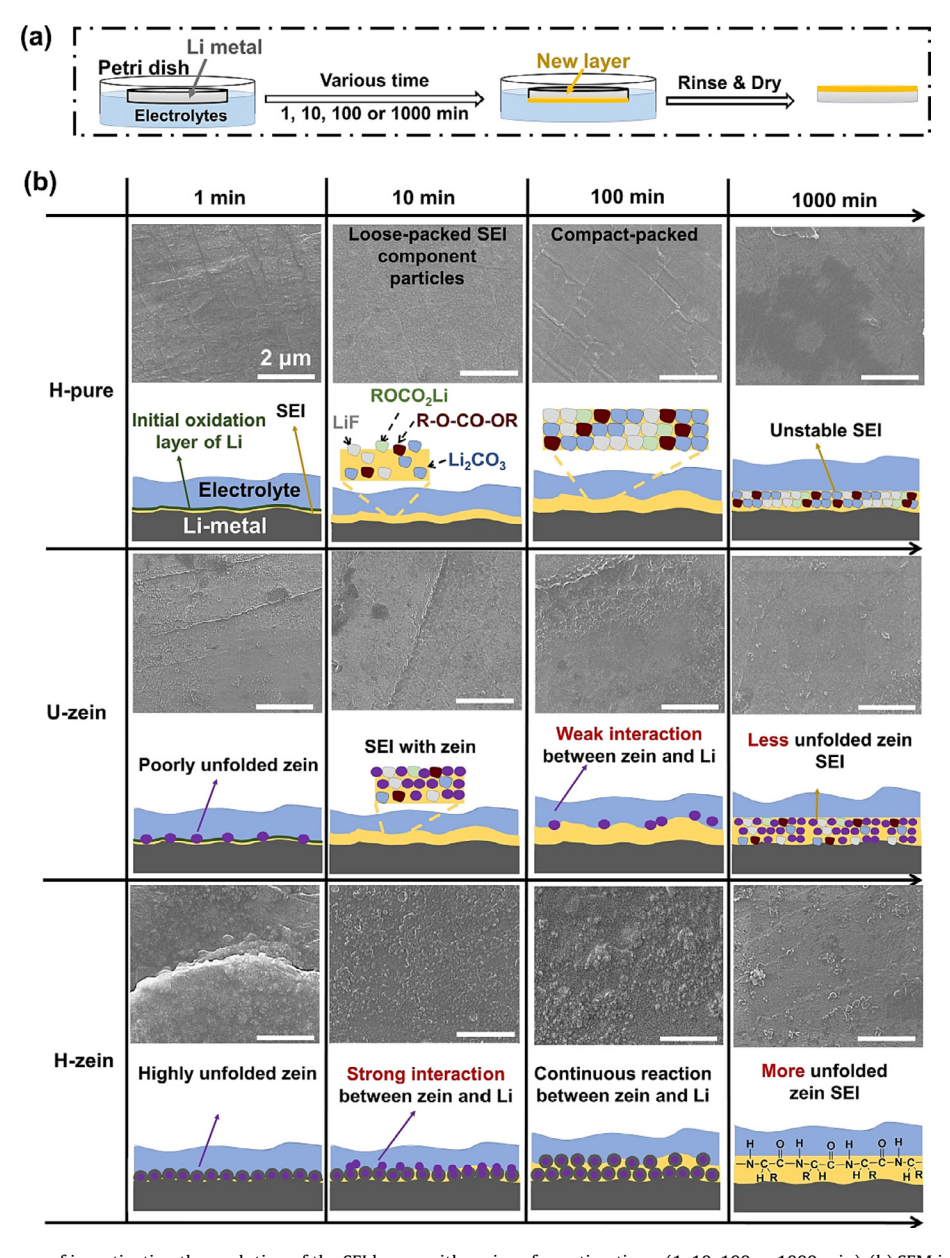


Fig. 4. (a) Experimental process of investigating the evolution of the SEI layers with various formation times (1, 10, 100 or 1000 min). (b) SEM images and the schematics of the SEI of H-zein, U-zein and H-pure with various formation time [32]. The polypeptides of zein protein, with a lower LUMO and a smaller bandgap compared to the electrolyte solvents [20], are inclined to firstly react with Li metal and form a zein-derived SEI on the surface. At the elevated temperature, due to the high reactivity and affinity between zein molecules and Li metal, Li will form a layer on zein nanoparticles and generate a zein@Li composites with core@shell structure at 1 min. With time, zein continues to react with Li at the interface of zein@Li composites, leading to the formation of a zein-derived SEI without zein particles core. By contrast, at ambient temperature, zein has low reactivity with Li and the zein nanoparticles adhered to the surface of Li, creating a zein-particle-contained SEI at 1000 min.

zein-modified SEI on Li metal can be clearly found at different formation time. At 1 min, a few protein nanoparticles are adhered to the Li metal of U-zein, whereas numerous protein nanoparticles with a Li shell that are inserted into Li metal surface can be found in H-zein, demonstrating the strong interaction between heattreated zein and Li due to the abundant exposed functional groups. At 10 and 100 min, the adhered zein particles and zein macromolecules in electrolyte continue to take part in the formation of SEI particles and be absorbed to the surface of Li, hence the SEI of U-zein is flatter at 10 min and more protein particles are found at 100 min. In sharp contrast, the H-zein SEI absorbs more zein particles and has a higher zein-Li reaction rate due to the richly exposed functional groups of highly unfolded zein, resulting in a zein nanoparticle layer at 10 min and smaller zein particles at 100 min. After the formation time of 1000 min, a flat zeinderived SEI formed on both U-zein and H-zein samples. The results demonstrate that the appropriate elevated temperature can improve the SEI formation speed and modify the morphology of SEI, thus reducing the stand-still time and optimizing the performance of final cells.

The contact angle measurement of electrolyte droplets on various SEIs is performed to investigate the wetting behavior of SEIs.

As shown in Fig. S9, for the U-pure SEI, the static-zone contact angles of SEI with various formation times (1 min, 10 min, 100 min and 1000 min) are 39.3°, 38.3°, 31.6° and 26.8°, respectively (Table S1). The enhanced wetting behavior by the increase of formation time may be because of the increasing content of lithium alkyl carbonates (ROCO₂Li) and Li₂CO₃ and LiF [33]. After heat treatment, the H-pure SEIs (Fig. 5a) with various formation times have the static-zone contact angles of 41.9°, 39.1°, 35.3° and 30.8°, respectively, which shows the same decreasing tendency, while smaller in value compared to U-pure SEIs, confirming that heat treatment does not have a big impact on wetting behavior of pure electrolyte derived SEI. After added zein, the wetting behavior of SEIs toward electrolyte has a great improvement (Fig. 5b and c). The static zone contact angle of U-zein and Hzein with various formation times decreased to 29.4°. 27.9°. 24.4°, 24.3° and 36.6°, 19.8, 22.8, 20.9°, respectively. This result indicates that at ambient temperature, zein takes part in the formation of U-zein SEIs in the first 100 min and participates in the growth of SEIs in the time range of 100-1000 min. Therefore, the contact angle of U-zein decreases from 1 min to 100 min and remains stable in 100-1000 min. While with heat treatment, the H-zein SEI forms rapidly in the first 10 min and remains nearly

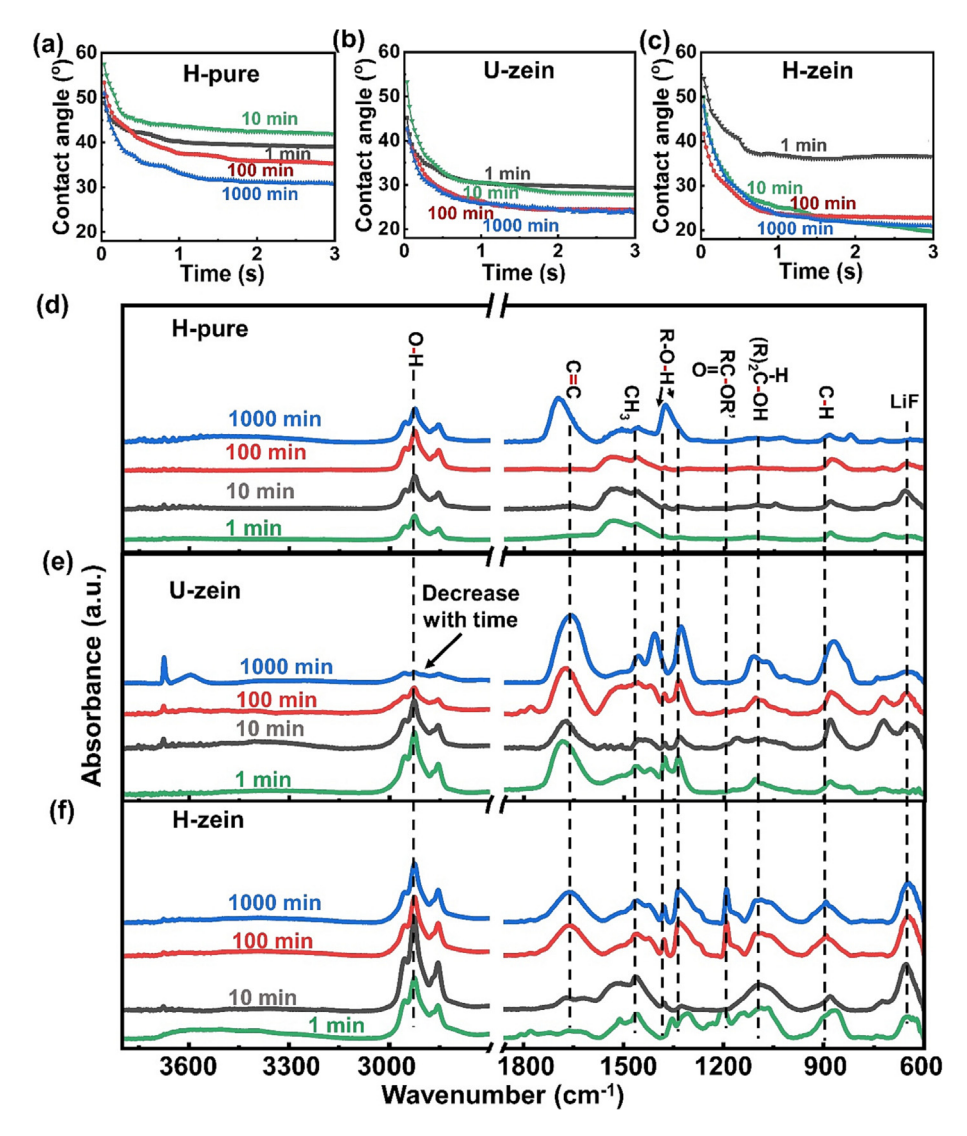


Fig. 5. Wetting behavior (with electrolyte) of various SEIs of H-pure (a), U-zein (b) and H-zein (c) with different treating times. ATR-FTIR of various SEIs of H-pure (d), U-zein (e) and H-zein (f) with different treating time.

unchanged after 10 min. Hence, the contact angle of H-zein has a large decrease from 1 min to 10 min and remains stable in 10–1000 min.

To reflect the evolution of chemical composition during the stand-still process of cells, FTIR of the SEIs with different formation times are tested. Fig S10 presents the U-pure SEI with various formation times. We can see that the functional groups keep nearly unchanged for the four SEIs with different formation times. The rich peaks of the U-pure SEIs may be due to the trace amount of remaining solvent (EC and EMC) that is hard to remove at ambient temperature. In contrast, the H-pure SEIs (Fig. 5d) have fewer peaks at the formation time of 1, 10 and 100 min but show two strong peaks (1692 and 1378 cm⁻¹) at the formation time of 1000 min. The appearance of the new strong peaks corresponds to the peaks of DME-derived SEI (Fig. S4), which is may be because the SEI of H-pure at 1000 min is much thicker than at 1, 10 and 100 min, therefore, trapping more DME molecules inside. After adding zein to the electrolyte, more peaks are found in the finger-

print region. Fig. 5(e) shows the U-zein SEIs with various formation times. Compared with U-pure SEIs, it can be found that the peak strength of intermolecular O-H bonding (2925 cm⁻¹) for U-zein SEI becomes weaker as the formation time increases. This result indicates that at ambient temperature, zein was poorly unfolded, hiding the abundant intramolecular O-H bonding inside and building weak intermolecular O-H bonding. In addition, zein participates in the formation of U-zein SEIs at a slow rate in the formation time of 0-1000 min, At 1000 min, the U-zein SEI impedes the reaction between DME and Li metal, leading to the weak strength of intermolecular O-H bonding peak at 2925 cm⁻¹. In sharp contrast with U-zein SEIs, H-zein SEIs (Fig. 5f) shows a stable strong peak of O-H bonding from 1 min to 1000 min, demonstrating the higher formation rate of zein modified SEI layer in the initial 1 min. The strong peak found at 650 cm⁻¹ of H-zein SEIs with various formation times can be ascribed to the formation LiF, indicating the anion trapping ability of the H-zein SEIs. Compared with H-pure, H-zein has more peaks

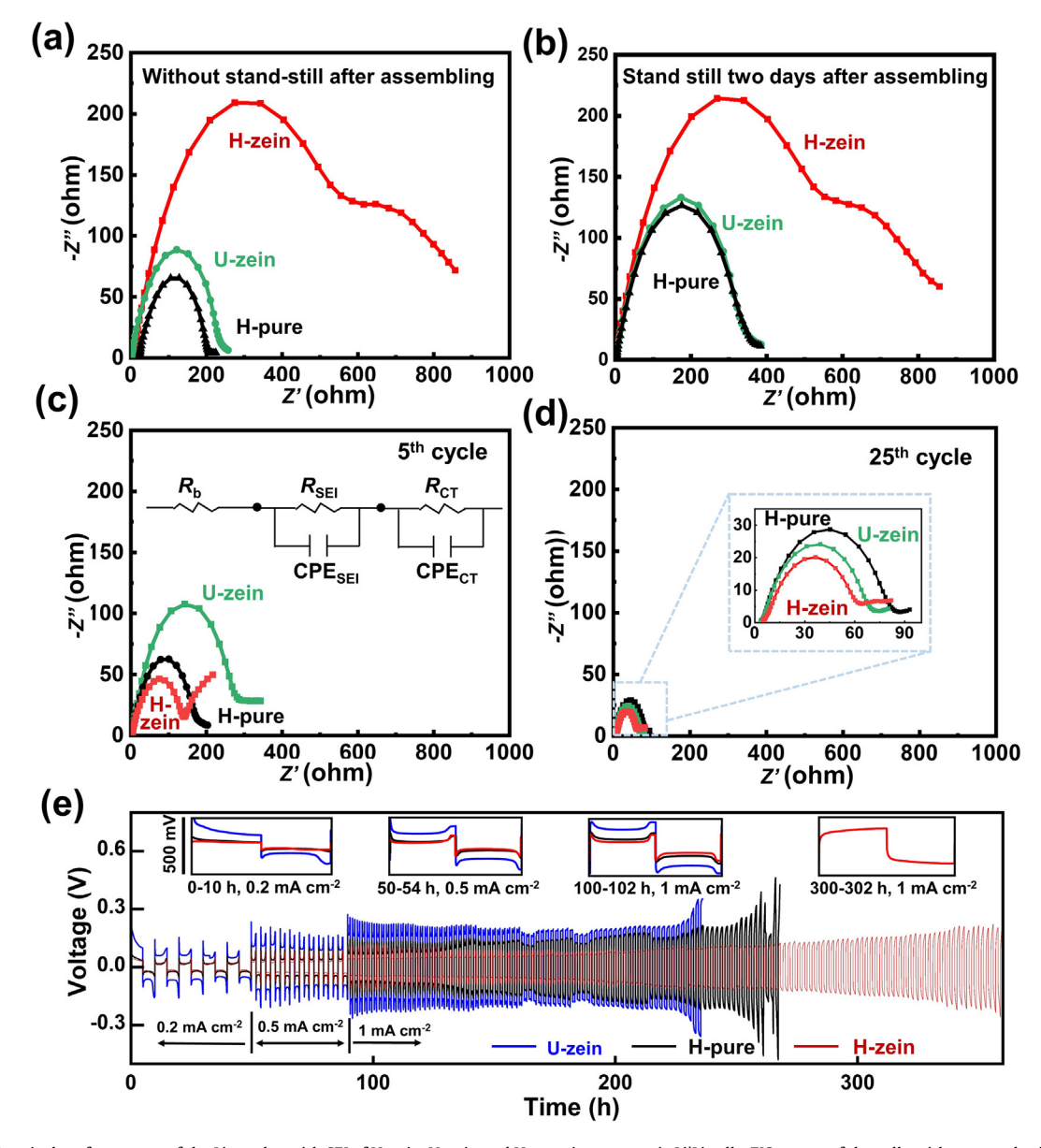


Fig. 6. Electrochemical performances of the Li anodes with SEI of H-zein, U-zein and H-pure in symmetric Li|Li cells. EIS curves of the cells without stand-still after assembling (a), stand still two days after assembling (b), after 5 cycles (c) and after 25 cycles (d). (e) Galvanostatic cycling of cells at various current densities (0.2, 0.5 and 1 mA cm⁻²) with a constant total capacity of 1 mAh cm⁻².

in the fingerprint area that correspond to various functional groups. The functional groups of H-zein SEIs are derived from the peptide chain of zein macromolecules. These results are due to the denatured structure of heated zein macromolecule that exposes abundant functional groups outside.

To further investigate the component differences between Uzein and H-zein SEIs, the Li metals with the SEI of various formation time were exposed to air for 24 h. The FTIR results of the oxidized Li plates are shown in Fig. S11. The strong peaks of intermolecular O–H bonding (2982 and 2902 cm⁻¹) can be found in all U-zein SEIs but are not shown in H-zein. The disappearance of O–H in H-zein may be because of the larger thickness of H-zein SEIs compared to U-zein. Moreover, the peak strength of Li₂-CO₃ (1405 and 858 cm⁻¹) of U-zein SEIs keeps unchanged, but that of H-zein SEIs becomes weaker as the formation time increases. The decreased ratio of Li₂CO₃ is due to the high content of zein in H-zein SEI after a long formation time. These results demonstrate that after the heat treatment, zein is denatured and participates in the formation of an SEI layer that is rich in more unfolded zein macromolecules.

3.3. Electrochemical performance of the Li with protein-modified SEIs

In order to characterize the resistance of various SEIs, Electrochemical Impedance Spectroscopy (EIS) analysis is performed in symmetric Li cells. To maintain the consistency of all cells, the electrolyte amount (40 uL) and assembling pressure (100 MPa) were strictly controlled. The intercept point along the real axis in highfrequency range is attributed to the bulk resistance (R_b). The large semicircle in the high and medium frequency range corresponds to the resistance of SEI layers. The small semicircle in the low frequency range represents the charge-transfer interfacial resistance $(R_{\rm CT})$. As shown in Fig. 6(a) and Table S2, at the initial state without stand-still after assembly of cells, H-zein cell has the largest $R_{\rm CT}$ (60.14 Ω) and $R_{\rm SEI}$ (563.8 Ω) compared to H-pure ($R_{\rm CT}$ = 28.34, $R_{\rm SEI}$ = 149.2 Ω) and U-zein cell ($R_{\rm CT}$ = 17.51, $R_{\rm SEI}$ = 209.9 Ω). This result is due to the large thickness of H-zein SEI that is induced by the high formation rate of SEI at an elevated temperature. After standing still in the ambient environment for two days (Fig. 6b and Tables S3), the R_{SEI} of H-zein remains nearly stable (579.8 Ω) while that of H-pure and U-zein has a large increase, which is 306.3 Ω and 310.8 Ω , respectively. This phenomenon demonstrates the stability of H-zein SEIs in the system of cells without cycling. The large decrease of R_{CT} for H-zein cell (35.04 Ω) compared to H-pure (22Ω) and U-zein (20.85Ω) cells is possibly due to the large thickness of H-zein SEI that is hard to be wetted by electrolytes in a short time. At the 5th cycle (Fig. 6c and Tables S4), the $R_{\rm SEI}$ of Hzein cell decreases to 122.9 Ω , which is smaller than that of Hpure (155.3 Ω) and U-zein (262.5 Ω) cells. This large decrease of impedance can be attributed to the reduction or oxidization of the functional groups in H-zein SEI. The R_{CT} of H-pure, U-zein and H-zein cells decrease to 12.11, 12.46 and 17.27, respectively. At the 25th cycle (Fig. 6d and Table S5), the $R_{\rm CT}$ of H-pure, U-zein and H-zein cells further decrease to 5.651, 5.056 and 6.04 Ω , respectively, and R_{SEI} decreases to 70.04, 59.13 and 52.2 Ω , respectively. The above results prove the formation of a zein-modified SEI with rich functional groups on the Li anode after heat treatment of zein macromolecules.

Fig. 6(e) shows the galvanostatic cycling of symmetrical Li cells using Li plates with various SEIs at various current densities of 0.2, 0.5 and 1 mA cm⁻² with the constant capacity of 1 mAh cm⁻². The H-zein cell exhibits a stable cycling performance over 360 h. In contrast, the H-pure and U-zein cells show short cycling performances that fail after 260 and 235 h, respectively. It is noted that the cells of U-pure and H-pure show nearly the same cycling life (Fig. S12). Therefore, the electrochemical performance of U-zein

cell was not included in the main text. To further investigate the evolution of the galvanostatic cycling, the cycling of cells at 0–10 h, 50–54 h, 100–102 h and 300–302 h are zoomed in and displayed as the inset in Fig. 6(e). For the cycling time of 0–10 h, 50–54 and 100–102 h with various current densities (0.2, 0.5 and 1 mA cm $^{-2}$), H-zein cell has polarizations (65.2, 57.6 and 94.2 mV) that are close to H-pure cell (76.8, 72.6 and 137.6 mV), respectively, while the U-zein cell has larger polarization (125.2, 227, and 320 mV), respectively. This result indicates that the heat treatment is critical for unfolding the zein macromolecule and forming a zein-modified SEI layer with rich functional groups.

To study the Li deposition after long-term cycling of cells with the various SEIs, the cycled Li plates disassembled from the cycled cells are characterized. SEM observation was employed to investigate the morphology of platted Li. As shown in Fig. 7(a and d), the plated Li anode of H-zein has a flat surface with nearly no pore on the surface. In comparison, the plated Li anode of U-zein (Fig. 7b) shows a cracked surface with more pores. The dead Li particles can be found in the cracked pores in the image with a large magnification (Fig. 7e). The plated Li anode with H-pure SEI is as shown in Fig. 7(c and f), a large amount of Li dendrites that are packed on the surface of the Li anodes can be clearly found, indicating the growth of Li dendrites during the plating process. The compositions of the cycled plated and stripped Li anodes with the various SEIs are determined by FTIR. As presented in Fig. 7(g), nearly all of the functional groups of cycled Li plates can be found in the uncycled Li plates with the various SEIs (Fig. 1c). Compared to the plated Li plate of U-zein and H-zein, the plated Li plate of Hzein has a strong peak of O-H at 2920 cm⁻¹, while this peak is not found in the stripped Li plate of H-zein. This phenomenon may be because of the transportation of small part of dissolved zein molecules through separator during the cycling process and adsorbed on the surface of plated Li surface [34]. In addition, the

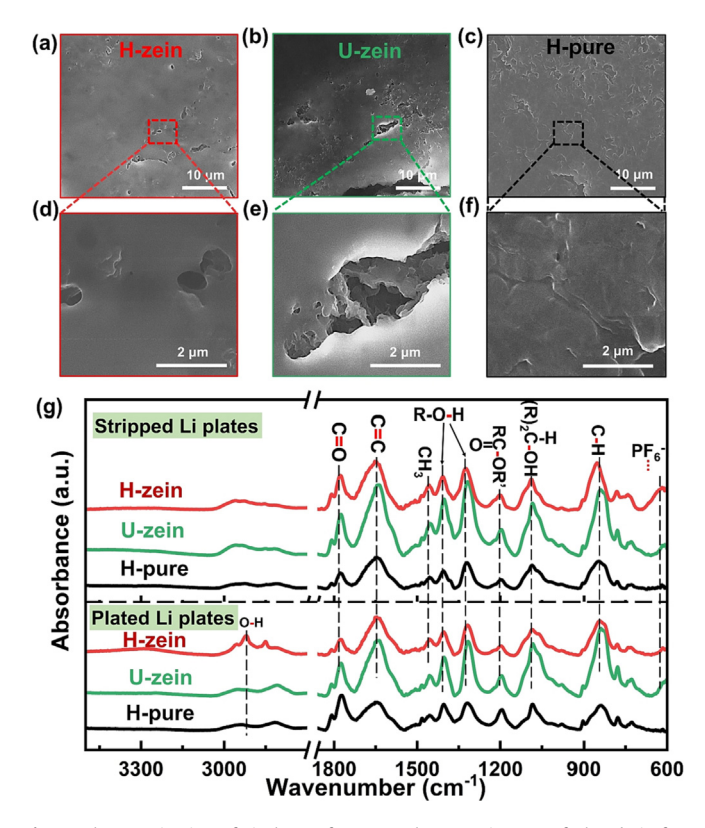


Fig. 7. Characterization of Li plates after 75 cycles. SEM images of plated Li of Hzein (a and d), U-zein (b and e) and H-pure (c and f). (g) FTIR results of the plated and stripped Li plates after 75 cycles.

stripped and plated Li plates of H-pure do not show an obvious peak for PF₆ at 610 cm⁻¹. In sharp contrast, the U-zein and H-zein both have a strong peak of PF₆, demonstrating the interaction between zein molecules and anions in zein-derived SEI layers. In our previous study based on a stand-still process of 50 °C, we found that the zein additive can form an SEI on the surface of Li due to the smaller LUMO and smaller bandgap compared to the electrolyte solvents (EC and EMC) [20]. The zein-derived SEI was found with abundant polar functional groups (e.g., C=O, C-O, COO⁻) by FTIR and X-ray photoelectron spectroscopy. Therefore, an even Li⁺ flux was induced by the SEI, and a homogenous Li deposition formed on Li anode, suppressing the growth of Li dendrites. The results of this study further confirm that the improved cycling performance of H-zein cells is led by the rich exposed functional groups, which are derived from the unfolded macromolecules of zein.

The cycling performance of the Li anodes with various SEIs is studied in LiFePO₄|Li full cells. Fig. 8(a-d) shows the charging/discharging profiles of the cells with Li anodes of various SEIs at

different current rates. The plateau of curves is enlarged to carefully study the polarization of cells. At 0.1C in the first cycle (Fig. 8a), the voltage polarization for H-zein cell is 0.068 V, which is smaller than H-pure (0.077 V) and U-zein (0.083 V). At 0.2C in the 5th cycle (Fig. 8b), the voltage polarization for H-zein cell slightly increases to 0.069 V, and that for H-pure and U-zein cells increase to 0.078 V and 0.084 V, respectively. At a higher rate of 0.5C in the 10th cycle (Fig. 8c), H-zein cell has a voltage polarization of 0.106 V that is still smaller than H-pure (0.116 V) and Uzein (0.114 V) cells. After long-term cycling of 200 cycles (Fig. 8d), the voltage polarization of H-zein cell is 0.2114 V, which is much smaller than the cell of U-zein (0.301 V) and H-pure. In specific, it can be seen that compared to the long-term cycling results of symmetrical cells (Fig. 5), the voltage polarization for Li anodes of U-zein is smaller than H-pure; while the voltage polarization for LiFePO₄|Li cell of U-zein is larger than that of H-pure. This is may be due to the modification of cathode electrolyte interphase (CEI) by zein molecules after long-time cycling. Fig. 8(e) and

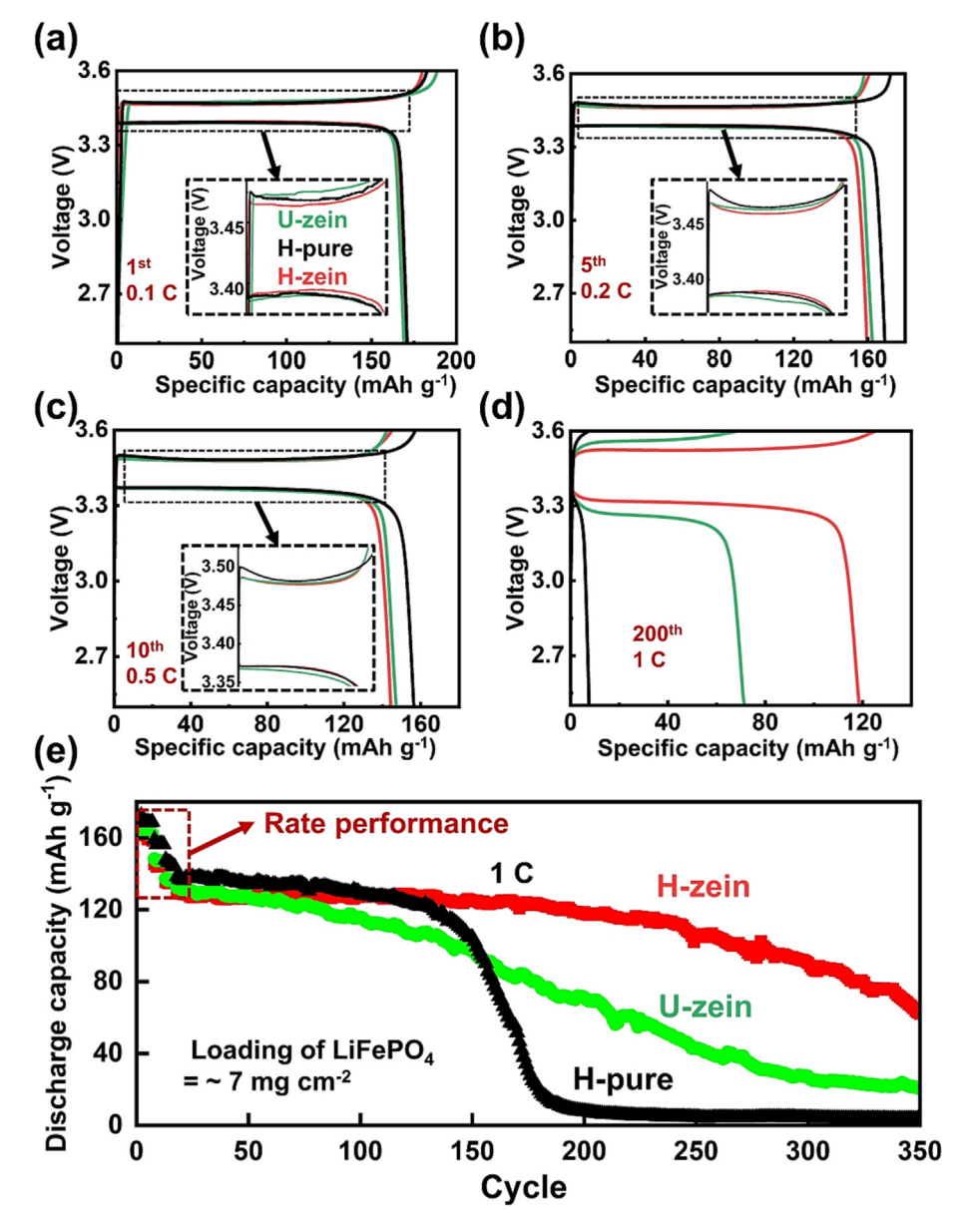


Fig. 8. (a–d) Charge and discharge curves of various cells at the 1st (a), 5th (b), 10th (c) and 200th (d) cycles. (e) Long-term cycling performance of the Li anodes with various SEIs in LiFePO₄|Li full cells.

Fig. S13 presented the long-term cycling performance of cells of various SEIs. The cell of H-zein shows excellent stability of cycling with a capacity of 118.5 mAh g^{-1} after 200 cycles, and the capacity retention is 70% (Fig. S14); while the cell of U-zein after 200 cycles has the capacity of 71 mAh g^{-1} that corresponds to the capacity retention of 42%, and H-pure cell has failed.

4. Conclusions

We investigate the formation of various protein-modified SEIs between Li anode and the most commercialized electrolyte, carbon ester electrolyte, at different stand-still temperatures and the evolution of SEIs is further studied by controlling the duration of the stand-still process after electrolyte filling. The simulation study indicates that zein (corn protein) as the additive in the electrolyte has a more unfolded configuration at the elevated denaturation temperature, but exhibits a poorly unfolded configuration at ambient temperature. The FTIR results indicate that the H-zein SEI formed at the elevated temperature presents more exposed functional groups than at ambient temperature, leading to an improved wetting behavior that is confirmed by the contact angle analysis. Therefore, for H-zein SEI, a higher formation rate is achieved, and becomes stable after a short-time stand-still process. As a result, the symmetrical Li|Li cell of H-zein achieves a prolonged cycling performance of >360 h and smaller polarization of 94.2 mV at 1 mA cm⁻² compared to the cell of U-zein with a cycling performance of \sim 260 h and polarization of 320 mV at 1 mA cm⁻². Moreover, the full cell of LiFePO₄|Li with the H-zein SEI exhibits a more stable long-term cycling performance with a capacity retention of 70% compared to 42% for the cell of U-zein after 200 cycles. Other proteins with rich polar functional groups and an appropriate denaturation processes also have the potential to improve the stability of Li anodes. This study will inspire future studies on the production process of LMBs toward their commercialization.

CRediT authorship contribution statement

Chenxu Wang: Writing - original draft, Investigation, Conceptualization, Formal analysis. Ryan Odstrcil: Writing - review & editing, Modeling. Jin Liu: Writing - review & editing, Supervision, Funding acquisition. **Wei-Hong Zhong:** Writing – review & editing, Supervision, Funding acquisition.

Declaration of competing interest

The authors declare that they have no known competing financial interests or personal relationships that could have appeared to influence the work reported in this paper.

Acknowledgments

This work was supported by NSF CBET 1929236. Computational resources were provided in part by the Extreme Science and Engineering Discovery Environment (XSEDE) under grant No. MCB170012. The authors would like to gratefully acknowledge the support for microscopy characterizations from the Franceschi Microscopy & Imaging Center at Washington State University.

Appendix A. Supplementary data

Supplementary data to this article can be found online at https://doi.org/10.1016/i.jechem.2022.06.017.

References

- [1] D. Lin, Y. Liu, Y. Cui, Nat. Nanotechnol. 12 (2017) 194-206.
- [2] J. Liu, Z. Bao, Y. Cui, E.J. Dufek, J.B. Goodenough, P. Khalifah, Q. Li, B.Y. Liaw, P. Liu, A. Manthiram, Y.S. Meng, V.R. Subramanian, M.F. Toney, V.V. Viswanathan, M.S. Whittingham, J. Xiao, W. Xu, J. Yang, X.Q. Yang, J.G. Zhang, Nat. Energy 4 $(2019)\ 180-186$
- [3] X.B. Cheng, R. Zhang, C.Z. Zhao, F. Wei, J.G. Zhang, Q. Zhang, Adv. Sci. 3 (2015)
- [4] Y. Liu, R. Zhang, J. Wang, Y. Wang, IScience 24 (2021) 102332.
- [5] A. Kwade, W. Haselrieder, R. Leithoff, A. Modlinger, F. Dietrich, K. Droeder, Nat. Energy 3 (2018) 290–300.
- [6] L.E. Camacho-Forero, T.W. Smith, S. Bertolini, P.B. Balbuena, J. Phys. Chem. C 119 (2015) 26828-26839.
- [7] H. Wu, H. Jia, C. Wang, J.G. Zhang, W. Xu, Adv. Energy Mater. 11 (2021) 1-35.
- [8] W. Huang, P.M. Attia, H. Wang, S.E. Renfrew, N. Jin, S. Das, Z. Zhang, D.T. Boyle, Y. Li, M.Z. Bazant, B.D. McCloskey, W.C. Chueh, Y. Cui, Nano Lett. 19 (2019) 5140-5148.
- [9] J. Ding, R. Xu, X. Ma, Y. Xiao, Y. Yao, C. Yan, J. Huang, Angew. Chemie 134 (2022)
- [10] X. Shan, Y. Zhong, L. Zhang, Y. Zhang, X. Xia, X. Wang, J. Tu, J. Phys. Chem. C 125 (2021) 19060-19080.
- [11] P. Keil, A. Jossen, J. Electrochem. Soc. 164 (2017) A6066-A6074.
- [12] S.J. An, J. Li, C. Daniel, D. Mohanty, S. Nagpure, D.L. Wood, Carbon N. Y. 105 2016) 52-76.
- [13] F. Single, A. Latz, B. Horstmann, ChemSusChem 11 (2018) 1950–1955.
- [14] P. Lu, C. Li, E.W. Schneider, S.J. Harris, J. Phys. Chem. C 118 (2014) 896–903.
- [15] P.M. Attia, S. Das, S.J. Harris, M.Z. Bazant, W.C. Chueh, J. Electrochem. Soc. 166 2019) E97-E106.
- [16] H. Zhang, G.G. Eshetu, X. Judez, C. Li, L.M. Rodriguez-Martínez, M. Armand, Angew. Chem. - Int. Ed. 57 (2018) 15002–15027.
- [17] M.T.F. Rodrigues, F.N. Sayed, H. Gullapalli, P.M. Ajayan, J. Power Sources 381 (2018) 107-115.
- W. Pfleging, J. Pröll, J. Mater. Chem. A 2 (2014) 14918-14926.
- [19] C.F.J. Francis, I.L. Kyratzis, A.S. Best, Adv. Mater. 32 (2020) 1904205.
 [20] C. Wang, X. Fu, C. Ying, J. Liu, W. Zhong, Chem. Eng. J. 437 (2022) 135283.
- [21] M. Chen, X. Fu, Z. Chen, J. Liu, W. Zhong 2006744 (2020) 1–25.
- [22] C. Wang, X. Fu, S. Lin, J. Liu, W.-H. Zhong, J. Energy Chem. 64 (2021) 485–495.
- [23] X. Fu, Y. Wang, X. Fan, L. Scudiero, W.H. Zhong, Small 14 (2018) 1803564.
 [24] M.J. Abraham, T. Murtola, R. Schulz, S. Páll, J.C. Smith, B. Hess, et al., GROMACS: High performance molecular simulations through multi-level parallelism from laptops to supercomputers, SoftwareX. 1-2 (2015) 19-25, https://doi.org/ 10.1016/j.softx.2015.06.001
- [25] W.L. Jorgensen, D.S. Maxwell, J. Tirado-Rives, Development and Testing of the OPLS All-Atom Force Field on Conformational Energetics and Properties of Organic Liquids, Journal of the American Chemical Society. 118 (45) (1996) 11225-11236, https://doi.org/10.1021/ja9621760.
- [26] G. Bussi, D. Donadio, M. Parrinello, Canonical sampling through velocity rescaling, The Journal of Chemical Physics. 126 (1) (2007), https://doi.org/ 10.1063/1.2408420 014101.
- [27] H.J.C. Berendsen, J.P.M. Postma, W.F. van Gunsteren, A. DiNola, J.R. Haak, Molecular dynamics with coupling to an external bath, The Journal of Chemical Physics. 81 (8) (1984) 3684–3690, https://doi.org/10.1063/1.448118.
- [28] M. Parrinello, A. Rahman, Polymorphic transitions in single crystals: A new molecular dynamics method, Journal of Applied Physics. 52 (12) (1981) 7182-7190, https://doi.org/10.1063/1.328693
- [29] W. Humphrey, A. Dalke, K. Schulten, VMD: Visual molecular dynamics, Journal of Molecular Graphics. 14 (1) (1996) 33-38, https://doi.org/10.1016/0263 7855(96)00018-5
- [30] D. van der Spoel, P.J. van Maaren, The Origin of Layer Structure Artifacts in Simulations of Liquid Water, J Chem Theory Comput. 2 (1) (2006) 1-11, https://doi.org/10.1021/ct0502256, PubMed PMID: 26626372.
- [31] N. Hameed, S.P. Thomas, R. Abraham, S. Thomas, Express Polym. Lett. 1 (2007) 345-355
- [32] X.-B. Cheng, R. Zhang, C.-Z. Zhao, F. Wei, J.-G. Zhang, Q. Zhang, X.B. Cheng, R. Zhang, C.Z. Zhao, F. Wei, Q. Zhang, J.-G. Zhang, Adv. Sci. 3 (2016) 1500213.
- [33] S. Jurng, Z.L. Brown, J. Kim, B.L. Lucht, Energy Environ. Sci. 11 (2018) 2600-
- [34] T. Wang, Y. Li, J. Zhang, K. Yan, P. Jaumaux, J. Yang, C. Wang, D. Shanmukaraj, B. Sun, M. Armand, Y. Cui, G. Wang, Nat. Commun. 11 (2020) 1-9.